JACS
JOURNAL OF THE AMERICAN CHEMICAL SOCIETY

ARTICLE

pubs.acs.org/JACS

# Design and Synthesis of Bimetallic Electrocatalyst with Multilayered Pt-Skin Surfaces

Chao Wang,[†] Miaofang Chi,[‡] Dongguo Li,[†,§] Dusan Strmcnik,[†] Dennis van der Vliet,[†] Guofeng Wang,[∥] Vladimir Komanicky,[†,¶] Kee-Chul Chang,[†] Arvydas P. Paulikas,[†] Dusan Tripkovic,[†] John Pearson,[†] Karren L. More,[‡] Nenad M. Markovic,[†] and Vojislav R. Stamenkovic*[,†]

[†]Materials Science Division, Argonne National Laboratory, Argonne, Illinois 60439, United States

[‡]Division of Material Science and Technology, Oak Ridge National Laboratory, Oak Ridge, Tennessee 37831, United States

[§]Department of Chemistry, Brown University, Providence, RI 02912, United States

[∥]Department of Mechanical Engineering and Materials Science, University of Pittsburgh, Pittsburgh, Pennsylvania 15260, United States

[¶]Safarik University, Faculty of Science, Kosice 04154, Slovakia

Supporting Information

**ABSTRACT:** Advancement in heterogeneous catalysis relies on the capability of altering material structures at the nanoscale, and that is particularly important for the development of highly active electrocatalysts with uncompromised durability. Here, we report the design and synthesis of a Pt-bimetallic catalyst with multilayered Pt-skin surface, which shows superior electrocatalytic performance for the oxygen reduction reaction (ORR). This novel structure was first established on thin film extended surfaces with tailored composition profiles and then implemented in nanocatalysts by organic solution synthesis. Electrochemical studies for the ORR demonstrated that after prolonged exposure to reaction conditions, the Pt-bimetallic catalyst with multilayered Pt-skin surface exhibited an improvement factor of more than 1 order of magnitude in activity versus conventional Pt catalysts. The substantially enhanced catalytic activity and durability indicate great potential for improving the material properties by fine-tuning of the nanoscale architecture.

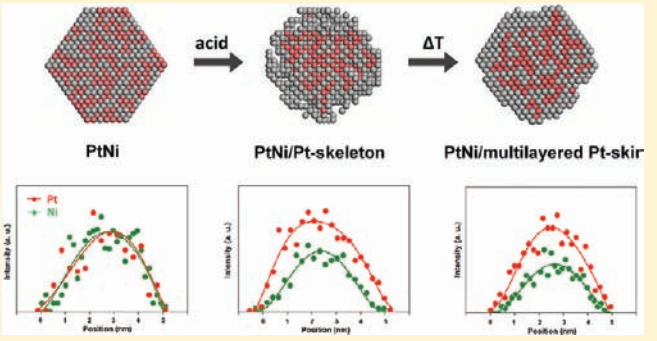


## INTRODUCTION

The foreground of sustainable energy is built up on a renewable and environmentally compatible scheme of chemical-electrical energy conversion. One of the key processes for such energy conversion is the electrocatalytic reduction of oxygen, the cathode reaction in fuel cells[1] and metal−air batteries,[2] where an electrocatalyst is used to accelerate the course of ORR. Current electrocatalysts used for this reaction are typically in the form of dispersed Pt nanoparticles (NPs) on amorphous high-surface-area carbon. Considering the high cost and limited resource of Pt, large-scale applications of these renewable energy technologies demand substantial improvement of the catalyst performance so that the amount of Pt needed can be significantly reduced. For example, a 5-fold improvement of catalytic activity for the ORR is required for the commercial implementation of fuel cell technology in transportation.[3]

Our recent work on well-defined extended surfaces has shown that high catalytic activity for the ORR can be achieved on Pt−bimetallic alloys ($Pt_3M$, M = Fe, Co, Ni, etc.), due to the altered electronic structure of the Pt topmost layer and hence reduced adsorption of oxygenated spectator species (e.g., $OH^-$) on the surface.[4] It was also found that in an acidic electrochemical environment the non-noble 3d transition metals are dissolved from the near-surface layers, which leads to the formation of Pt-skeleton surfaces. Moreover, the thermal treatment of $Pt_3M$ alloys in ultra high vacuum (UHV) has been shown to induce segregation of Pt and formation of a distinctive topmost layer that was termed Pt-skin surface. However, the same treatment did not cause Pt to segregate over PtM alloys with high content (≥50%) of non-Pt elements.[4b,5] Recently, we further demonstrated the surfacing of an ordered Pt(111)-skin over $Pt_3Ni(111)$ single crystal with 50% of Ni in the subsurface layer. This unique nanosegregated composition profile was found to be responsible for the dramatically enhanced ORR activity.[6]

On the basis of these findings, it could be envisioned that the most advantageous nanoscale architecture for a bimetallic electrocatalyst would correspond to the segregated Pt-skin composition profile established on extended surfaces. A lot of effort has thus been dedicated,[7] but it still remains elusive, to finely tune the Pt-bimetallic nanostructure to achieve this desirable surface structure and composition profile. Major obstacles reside not only in the difficulty to manipulate elemental distribution at the nanoscale, but also in the fundamental differences in atomic

**Received:** May 24, 2011
**Published:** July 19, 2011

  

structures, electronic properties, and catalytic performance between extended surfaces and confined nanomaterials. For example, in an attempt to induce surface segregation, high-temperature (>600 °C) annealing is typically applied for Pt-based alloy nanocatalysts. While improvement in specific activity is obtained, such treatment usually causes particle sintering and loss of electrochemical surface area (ECSA).[7b,8] Besides that, the surface coordination of nanomaterials is quite different from that of bulk materials; that is, the surface of NPs is rich in corner and edge sites, which have a smaller coordination number than the atoms on long-range ordered terraces of extended surfaces.[9] These low-coordination surface atoms are considered as preferential sites for the adsorption of oxygenated spectator species (e.g., $OH^-$)[10] and thus become blocked for adsorption of molecular oxygen and inactive for the ORR.[9b,11] Additionally, due to strong Pt−O interaction, these sites are more vulnerable for migration and dissolution, resulting in poor durability and fast decay of the catalyst.[12] The latter effect is even more pronounced in Pt−bimetallic systems, considering that more undercoordinated atoms are present on the skeleton surfaces formed after the depletion of nonprecious metals from near-surface regions.[4a,13] Therefore, a systematic approach with all of these factors integrally considered becomes necessary to pursue the design and synthesis of advanced bimetallic catalysts.

Our focus in this study has been placed on the fine-tuning of Pt−bimetallic nanostructure aiming to achieve the advantageous Pt-skin surface structure and composition profile established on extended surfaces. We started with Pt thin films of controlled thickness deposited over PtNi substrate to explore the correlation between the surface composition profile and catalytic performance. These findings were then applied for guiding the synthesis of nanocatalysts with the optimized structure. The outcome of such effort is an advanced Pt−bimetallic catalyst with altered nanoscale architecture that is highly active and durable for the ORR.

## EXPERIMENTAL SECTION

**Thin Film Preparation.** Pt films were deposited at room temperature on PtNi substrates (6 mm in diameter), which were set 125 mm away from DC sputter magnetrons in 4 mTorr argon gas (base vacuum $1 \times 10^{-7}$ Torr). The Pt source rate (0.32 Å/s) was determined by quartz crystal microbalance, and an exposure duration of 7.0 s was calibrated for the nominal thickness of 2.2−2.3 Å for a monolayer of Pt. The film thickness was derived from the exposure time of computer-controlled shutters during sputtering.

**NP and Catalyst Synthesis.** In a typical synthesis of PtNi NPs, 0.67 mmol of $Ni(ac)_2 \cdot 4H_2O$ was dissolved in 20 mL of diphenyl either in the presence of 0.4 mL of oleylamine and 0.4 mL of oleic acid. 0.33 mmol of 1,2-tetradodecanediol was added, and the formed solution was heated to 80 °C under Ar flow. After a transparent solution formed, the temperature was further raised to 200 °C, where 0.33 mmol of $Pt(acac)_2$ dissolved in 1.5 mL of dichlorobenzene was injected. The solution was kept at this temperature for 1 h and then cooled to room temperature. An amount of 60 mL of ethanol was added to precipitate the NPs, and the product was collected by centrifuge (6000 rpm, 6 min). The obtained NPs were further washed by ethanol two times and then dispersed in hexane. The as-synthesized PtNi NPs were deposited on high surface area carbon (~900 $m^2/g$) by mixing the NPs with carbon black (Tanaka, KK) in hexane or chloroform with a 1:1 ratio in mass. This mixture was sonicated for 1 h and then dried under nitrogen flow. The organic surfactants were removed by thermal treatment at 150−200 °C in an oxygenated atmosphere. The obtained catalyst is denoted as "as-prepared PtNi/C". For the acid treatment, ~10 mg of the as-prepared PtNi/C catalyst was mixed with 20 mL of 0.1 M $HClO_4$ that has been used as electrolyte in electrochemical measurements. After overnight exposure to the acidic environment, the product was collected by centrifuge and washed three times by deionized water. Such NPs are named as "acid treated PtNi/C". The acid treated PtNi/C was further annealed at 400 °C to reduce low-coordinated surface sites, and the obtained catalyst is termed as "acid treated/annealed PtNi/C".

**Microscopic Characterization.** TEM images were collected on a Philips EM 30 (200 kV) equipped with EDX functionality. XRD patterns were collected on a Rigaku RTP 300 RC machine. STEM and elemental analysis were carried out on a JEOL 2200FS TEM/STEM with a CEOS aberration (probe) corrector. The microscope was operated at 200 kV in HAADF-STEM mode equipped with a Bruker-AXS X-Flash 5030 silicon drift detector. The probe size was ~0.7 Å and the probe current was ~30 pA during HAADF-STEM imaging. When accumulating EDX data, the probe current was increased to ~280 pA and the probe size was ~2 Å. The presented EDX data were confirmed to be from "e-beam damage-free" particles by comparing STEM images before and after EDX acquisition.

**X-ray Absorption Spectroscopy.** X-ray fluorescence spectra of at the Ni K and Pt $L_3$ edges were acquired at bending magnet beamline 12-BM-B at the Advanced Photon Source (APS), Argonne National Laboratory. The incident radiation was filtered by a Si(111) double-crystal monochromator (energy resolution $\Delta E/E = 14.1 \times 10^{-5}$) with a double mirror system for focusing and harmonic rejection.[14] All of the data were taken in fluorescence mode using a 13-element Germanium array detector (Canberra), which was aligned with the polarization of the X-ray beam to minimize the elastic scattering intensity. Co and Ge filters (of 6 absorption length in thickness) were applied in front of the detector to further reduce the elastic scattering intensity for the Ni K and Pt $L_3$ edges, respectively. The Ni K and Pt $L_3$ edge spectra were calibrated by defining the zero crossing point of the second derivative of the XANES spectra for Ni and Pt reference foils as 8333 and 11564 eV, respectively. The background was subtracted using the AUTOBK algorithm,[15] and data reduction was performed using Athena from the IFEFFIT software suite.[16] A scheme of the homemade *in situ* electrochemical cell and setup at beamline was shown in the Supporting Information, Figure S9.

**Electrochemical Characterization.** The electrochemical measurements were conducted in a three-compartment electrochemical cell with a rotational disk electrode (RDE, 6 mm in diameter) setup (Pine) and a Autolab 302 potentiostat. A saturated Ag/AgCl electrode and a Pt wire were used as reference and counter electrodes, respectively. 0.1 M $HClO_4$ was used as electrolyte. The catalysts were deposited on glassy carbon electrode substrate and dried in Ar atmosphere without using any ionomer. The loading was controlled to be 12 $\mu g_{Pt}/cm^2_{disk}$ for PtNi/C nanocatalysts. All of the potentials given in the discussion were against reversible hydrogen electrode (RHE), and the readout currents were recorded with ohmic *iR* drop correction during the measurements.[17]

## RESULTS AND DISCUSSION

Pt films of various thicknesses, that is, 1−7 atomic monolayers (ML), were deposited in a vacuum by sputtering on PtNi (Pt:Ni = 1:1) substrate and then transferred to an electrochemical cell for further characterizations (see the Experimental Section). The as-sputtered Pt films consist of randomly distributed Pt nanoclusters (<1 nm), which mimic the Ni depleted Pt-skeleton structures.[4a] The film thickness was varied to explore the dependence of catalytic activity on the surface depletion depth in Pt-skeleton type of surfaces.[13] The choice of PtNi substrate was based on our previous results from nanosegregated extended surfaces[6] and most recent findings related to composition-dependent electrochemical properties of $Pt_xNi_{1-x}$ NPs,[13]

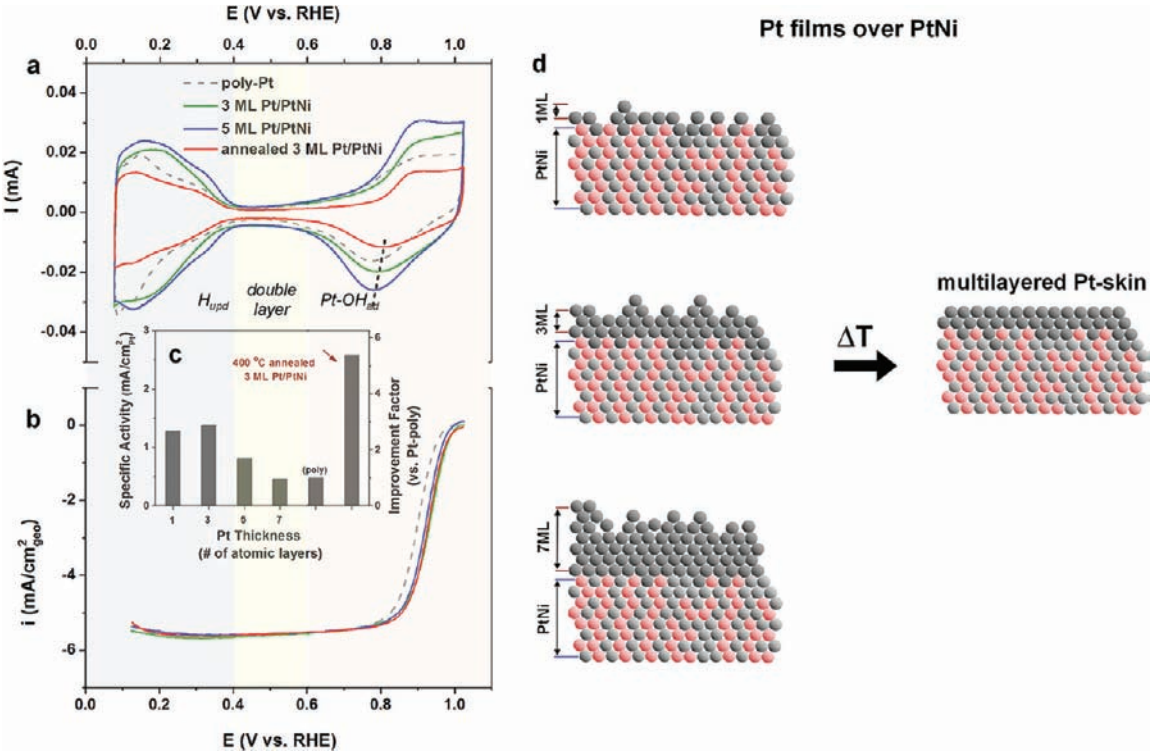


**Figure 1.** Electrochemical studies on the Pt thin films deposited over PtNi substrate by RDE: (a) cyclic voltammograms, (b) polarization curves, and (c) summary of specific activities and corresponding improvement factors (vs polycrystalline Pt surface) for the Pt films of various thicknesses. Cyclic voltammograms were recorded in Ar saturated 0.1 M $HClO_4$ electrolyte with a sweeping rate of 50 mV/s. Polarization curves were recorded in the same electrolyte under $O_2$ saturation with a sweep rate of 20 mV/s. Specific activities were presented as kinetic currents normalized by ECSAs obtained from integrated $H_{upd}$, except that for the annealed 3 ML Pt/PtNi surface which was based on $CO_{ad}$ stripping polarization curve.

which had confirmed the superior catalytic properties of systems with 50% of Ni in subsurface layers. Figure 1 summarizes the results of electrochemical studies for these thin films by rotating disk electrode (RDE). Cyclic voltammograms (CVs, Figure 1a) of the as-sputtered films correspond to polycrystalline Pt (poly-Pt) with similar, but slightly enlarged, underpotentially deposited hydrogen ($H_{upd}$) regions ($E$ < 0.4 V) due to the rougher surfaces. Consistent with our previous findings,[6] the onset of Pt−$OH_{ad}$ formation has anodic shifts for most of the Pt films (≤5 ML) as compared to poly-Pt (more visible in the CVs shown in the Supporting Information, Figure S1, with currents normalized by the electrochemical surface area (ECSA) obtained from integrated $H_{upd}$ region). Correspondingly, similar positive shifts are also present in the polarization curves for the ORR (Figure 1b). The largest shift of ∼30 mV was obtained for the Pt films with thicknesses of three atomic layers. Measured specific activities at 0.95 V, expressed as kinetic current normalized by the ECSA, show that the thinner films (≤3 ML) have improvement factors of ∼2.5 versus poly-Pt surface, which is in line with the previous results on polycrystalline $Pt_3M$ bulk alloys with the skeleton type of surfaces.[4b] Reduced enhancement was observed for thicker Pt films, for example, improvement factor of 1.7 for 5 ML of Pt, while the specific activity measured for the 7 ML film was close to that of poly-Pt. It should be noted here that for the as-sputtered films, 1 ML of Pt may not be able to entirely cover Ni atoms in the alloy substrate and protect them from dissolution, whereas addition of a second and/or third layer can effectively diminish this process. Along the same lines, this may also be the reason that the surfaces with 2 or 3 ML of Pt were found to be more active than that with 1 ML. These findings revealed that bimetallic systems with Pt-skeleton near-surface formation of up to three atomic layers in thickness are also capable of efficiently harvesting the beneficial properties of bimetallic alloys, while protecting the subsurface Ni from leaching out.

Because the as-sputtered skeleton type of surfaces have abundant low-coordination sites[4a] that are detrimental to the ORR, we have applied thermal treatment to investigate potential surface restructuring and further catalytic improvement. A moderate temperature of ∼400 °C was chosen as it was determined to be optimal for Pt−bimetallic nanocatalysts.[8a] In Figure 1a, the CV of annealed 3 ML Pt/PtNi surface is also shown. The suppressed $H_{upd}$ region and an even larger positive shift of the Pt−$OH_{ad}$ peak (Figure S1) indicates the formation of Pt-skin type of surface, which is smoother and less oxophilic with significantly reduced number of low-coordination surface atoms.[5,6] Additional proof of the transition toward Pt-skin is provided by the measured boost in specific activity for the ORR (Figure 1c), reaching an improvement factor of more than 5 with respect to poly-Pt (Figure 1d). Moreover, this high catalytic activity was based on the ECSA estimated from CO stripping polarization curves, not $H_{upd}$. The ECSA estimated from integrated $H_{upd}$ charge was found to be substantially smaller than that obtained from the electrochemical oxidation of adsorbed CO monolayer (Figure S2), which was not observed on unannealed Pt-skeleton surfaces. Such a difference can only be interpreted in terms of the altered electronic properties of the Pt-skin surface

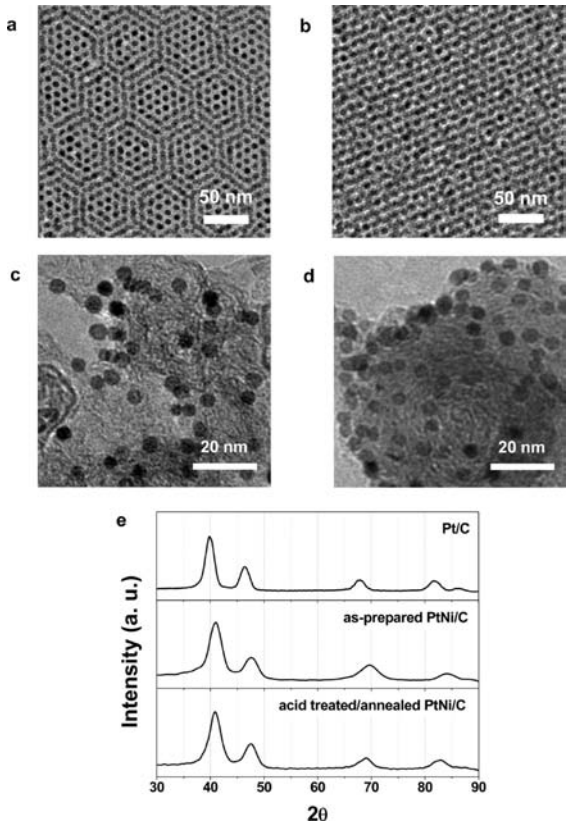


**Figure 2.** Representative transmission electron microscopy (TEM) images for (a,b) the as-synthesized PtNi NPs, (c) the as-prepared, and (d) the acid treated/annealed PtNi/C catalysts. (d) X-ray diffraction (XRD) patterns for the PtNi/C catalysts in comparison with commercial Pt/C (~6 nm in particle size).

that have affected the adsorption of hydrogenated species, but not the Pt−$CO_{ad}$ interaction.[6]

The above studies of Pt thin films over PtNi substrate, as well as the knowledge previously acquired from poly-/single-crystalline surfaces[4−6] and nanocatalysts,[8a,11b,13] have led us to a novel approach toward the design and synthesis of Pt−bimetallic catalysts with Pt terminated surfaces. The initial step in this approach should involve the synthesis of monodisperse and homogeneous PtNi NPs followed by intentional depletion of Ni from the surface, producing a skeleton type of surface structure. The final step is supposed to be the thermal treatment aimed to induce the transition from Pt-skeleton into Pt-skin type of structure by surface relaxation and restructuring. For that purpose, PtNi NPs were synthesized by simultaneous reduction of platinum acetylacetonate, $Pt(acac)_2$, and nickel acetate, $Ni(ac)_2$, in an organic solution (see the Experimental Section).[13,18] Figure 2a and b shows representative transmission electron microscopy (TEM) images of the as-synthesized PtNi NPs prepared with a molar ratio of 1:2 between the Pt and Ni precursors. The NP size was controlled to be ~5 nm[11b] with a very narrow size distribution, as evidenced by the formation of various types of super lattices after drying the nanoparticle suspension (in hexane) under ambient conditions.[19] The final composition was characterized by energy-dispersive X-ray spectroscopy (EDX), which confirmed an atomic ratio of Pt/Ni ≈ 1/1 (Figure S3). The as-synthesized NPs were incorporated into carbon black (~900 $m^2/g$) via a colloidal-deposition method, and the organic surfactants were efficiently removed by thermal treatment.[11b] Such as-prepared PtNi/C catalyst was first treated by acid to dissolve the surface Ni atoms[13] (Figure S3) and then annealed at 400 °C. These consecutive treatments were expected to bring on the Pt-skin type of surface over the substrate with 50% of Ni, which otherwise would not be possible because complete segregation of Pt only takes place in $Pt_3M$ systems.[5] TEM images of the acid treated/annealed catalyst do not show notable changes in morphology (Figure 2c and d), except a slight decrease (~0.3 nm) in average particle size (Figures S4). Additionally, X-ray diffraction (XRD) analysis was used to characterize the crystal structure of the NPs. As compared to the commercial Pt/C catalyst (Tanaka, ~6 nm), both the as-prepared and the acid treated/annealed PtNi/C systems show a face-centered cubic (fcc) pattern with noticeable shifts (e.g., ~1° for (111) peak) toward high angle (Figure 2e), corresponding to a decrease of lattice constant due to alloying between Pt and Ni.[20] The XRD pattern of the acid treated/annealed NPs has sharper peaks as compared to the as-prepared one, which indicates the increased crystallinity after annealing. These observations, in addition to the absence of peaks for separate Pt or Ni phases, show that the bimetallic catalyst preserved the alloy properties after the applied treatments.

The nanostructures and composition profiles of the PtNi/C catalysts were characterized by atomically resolved aberration-corrected high angle annular dark field-scanning transmission electron microscopy (HAADF-STEM) in combination with energy dispersive X-ray spectroscopy (EDX). Figure 3a shows representative HAADF-STEM images taken along the ⟨110⟩ zone axis of the as-prepared (left), acid treated (middle), and acid treated/annealed (right) PtNi/C catalysts, with the intensity profiles along ⟨001⟩ directions across the single particles shown in Figure 3b. As compared to the benchmark intensity profiles calculated for ideal octahedral alloy NPs of the same size and orientation (see the Supporting Information), NP exposed to acid shows 3−4 peaks on each side stretching above the standards, indicating the formation of a Pt-rich overlayer. This feature was preserved after annealing, but with 2−3 Pt-rich peaks on each side, corresponding to a reduced Pt overlayer thickness due to restructuring and smoothing (Figure 3b). These findings were further confirmed by EDX analysis. By scanning the e-beam across the particle while simultaneously analyzing the generated X-rays, composition line profiles were obtained for the NPs (Figure 3c). It can be seen that the distribution of Pt and Ni in the as-prepared catalyst was highly intermixed and the sketched trend lines were almost identical, indicating a homogeneous alloy nature of the catalyst particles. The treated catalysts have substantially broader distribution of Pt than Ni, with a difference of ~1 nm (at the half-maximum of the trend lines) for the acid treated and ~0.6 nm for the acid treated/annealed catalyst. Hence, both the intensity and the composition line profiles show that multilayered Pt-rich surface structure was formed by acid treatment and preserved after annealing.

The microscopic characterizations strongly point toward surface restructuring in the bimetallic catalyst upon annealing. This was additionally depicted by atomistic simulation of the nanostructure evolution subject to the acid and annealing treatments (Figure 3d for overviews and Figure 3e for cross-section views; see the Supporting Information for more details). It shows that removing Ni atoms from the surface led to the formation of a Pt-skeleton overlayer with a thickness of up to 3 atomic layers. Further relaxation of low-coordination surface atoms resulted in a multilayered Pt-skin surface, whereas the PtNi core was barely affected. It is important to mention that the relaxation process is expected to induce preferential formation of highly active (111) surface[6] (labeled by arrows in

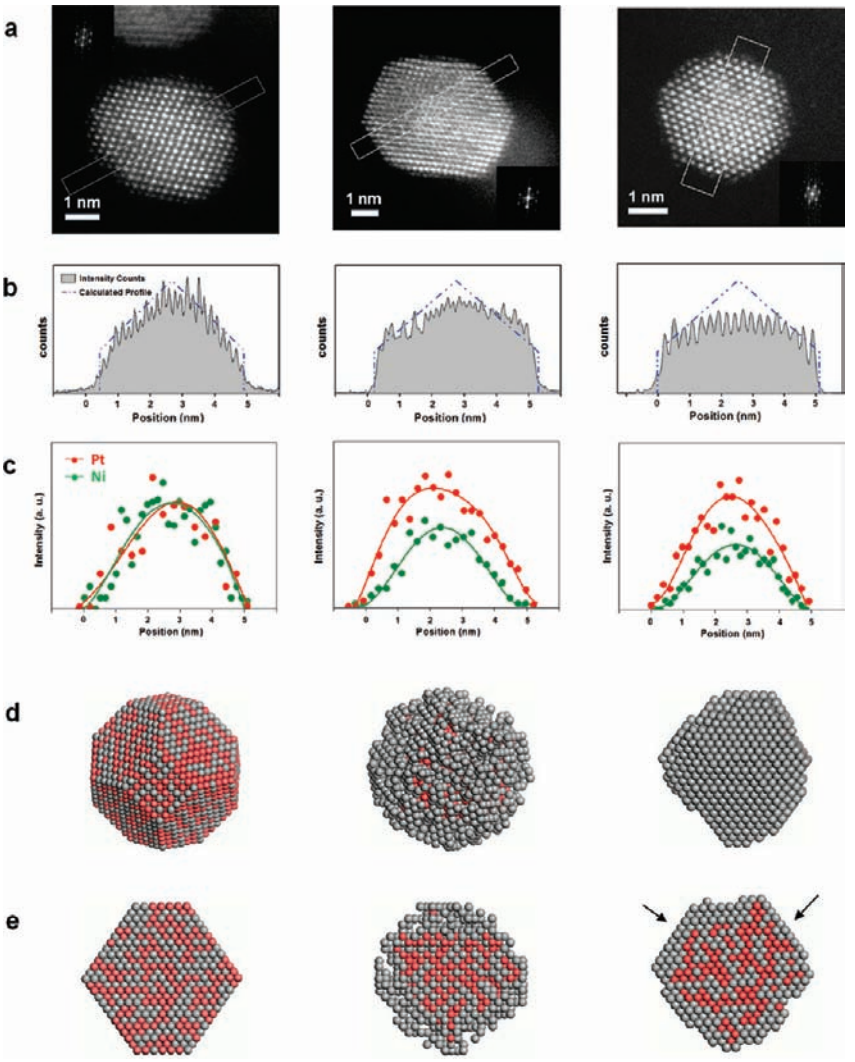


**Figure 3.** Microscopic characterization and theoretical simulation of nanostructure evolution in the PtNi/C catalysts: (a) Representative high-angle annular dark-field scanning transmission electron microscopy (HAADF-STEM) images taken along the zone axis ⟨110⟩, as confirmed by the fast Fourier transfer (FFT) patterns of the STEM images (shown as insets); (b) background subtracted, normalized intensity line profiles extracted for the regions marked in (a); (c) composition line profiles (normalized for Pt−L peaks) obtained by energy-dispersive X-ray spectroscopy (EDX) with an electron beam (∼2 Å in spot size) scanning across individual catalyst particles; (d) overview; and (e) cross-section views of the nanostructures depicted by atomistic particle simulation. The figure is also organized in columns for the as-prepared (left), acid treated (middle), and acid treated/annealed (right) PtNi/C catalysts, respectively.

Figure 3e), due to the higher atomic coordination, that is, lower surface energy, of this facet as compared to others.

To gain more insights into the nanostructure evolution, especially the correlation of surface structures to their electrochemical properties, we have carried out *in situ* X-ray absorption near edge structure (XANES) studies of the nanocatalysts (see the Experimental Section and Supporting Information for details). Figure 4a and b shows the normalized XANES spectra collected at Ni K and Pt $L_3$ edges, under the ORR-relevant conditions (∼1.0 V). As compared to the spectra of reference foils, Pt and Ni edge positions were found to correspond to the bulk oxidation state of zero for both elements in the treated catalysts.[21] It is intriguing to see that the acid treated catalyst shows higher white line intensity than does the acid treated/annealed catalyst at the Ni edge, which is caused by the presence of a small amount of NiO underlying the highly corrugated Pt-skeleton surface morphology in the acid treated catalyst,[22] whereas subsurface Ni in the acid treated/annealed catalyst was well protected. The distinction in surface structure between the two treated catalysts is even more visible at the Pt edge, where a slightly lower white line intensity for the acid treated/annealed catalyst corresponds to a reduced amount of platinum oxides under the same conditions, and, more fundamentally, less oxophilic surface with larger average surface coordination number.[5,22a,23] The findings from XANES provide additional evidence for the formation of surface relaxed multilayered Pt-skin in the acid treated/annealed catalyst and its superiority in protecting the inner Ni from leaching out.

On the basis of these results, we have managed to achieve the desirable nanoscale architecture established on PtNi supported Pt films, that is, multilayered Pt-skin over a particle core with 50% of Ni. Considering what was revealed from the studies on extended surfaces, the obtained nanocatalyst should show superior catalytic performance for the ORR, which was examined by RDE

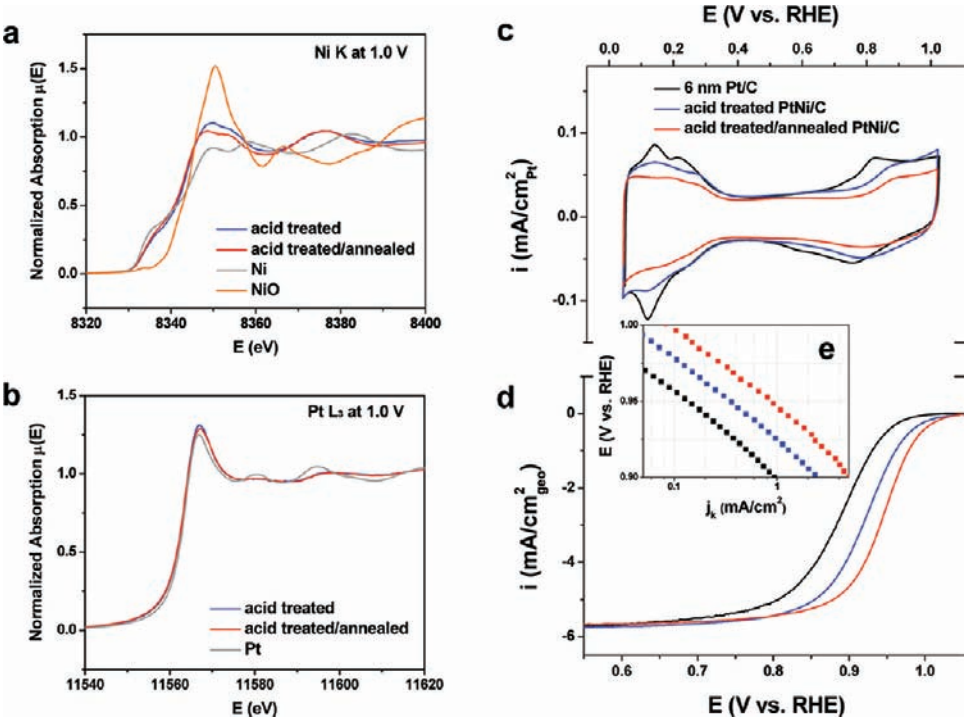


**Figure 4.** *In situ* X-ray absorption and electrochemical studies of the PtNi/C catalysts. (a,b) XANES spectra for the PtNi/C catalysts recorded at Ni K and Pt $L_3$ edges with an electrode potential of 1.0 V, in comparison with standard spectra of Ni, NiO, and Pt. (c) Cyclic voltammograms, (d) polarization curves, and (e) Tafel plots with the specific activity ($j_k$, kinetic current density) as a function of electrode potential, in comparison with the commercial Pt/C catalyst. Estimation of ECSA was based on integrated $H_{upd}$ for the Pt/C and acid treated PtNi/C catalysts, and $CO_{ad}$ stripping polarization curve for the acid treated/annealed PtNi/C catalyst.

measurements (see the Experimental Section). Figure 4c−e summarizes the electrochemical studies for the three types of nanocatalysts. It can be seen from the voltammograms (Figure 4c) that the $H_{upd}$ region ($E$ < 0.4 V) of the acid treated/annealed catalyst is largely suppressed versus the acid treated sample. On the positive side of the potential scale, the onset of oxide formation for the acid treated/annealed catalyst is shifted positively by about 20 mV versus that for the acid treated catalyst, and more than 50 mV with respect to Pt/C. Similar shifts are also seen for the reduction peaks in the cathodic scans. Such peak shifts are representative of a less oxophilic catalyst surface due to the formation of multilayered Pt-skin structure, and further corresponding to remarkable enhancement in the ORR activity as evidenced by the polarization curves shown in Figure 4d and the Tafel plots, Figure 4e. These findings are reminiscent of those on extended surfaces (Figure 1) and from *in situ* XANES studies (Figure 4b). At 0.95 V, the specific activity of the acid treated/annealed PtNi/C reaches 0.85 mA/cm$^2$, as compared to 0.35 mA/cm$^2$ for the acid treated specimen and 0.13 mA/cm$^2$ for Pt/C. This translates into improvement factors versus Pt/C of 3 and over 6 for the acid treated and acid treated/annealed PtNi/C catalysts, respectively, which is also in line with the results obtained on extended surfaces (Figure 1c). Therefore, the electrochemical studies of nanocatalysts validated that the scheme of the near surface architecture established on extended surfaces had been successfully applied to nanocatalysts by forming a multilayered Pt-skin surface. Remarkably, the ECSA of this catalyst obtained from integrated $H_{upd}$ region was over 30% lower than that from CO stripping (Figure S2), which also confirms the formation of Pt-skin type of surface in the nanocatalyst.

Moreover, the developed Pt−bimetallic catalyst with the unique nanoscale architecture does not only show enhanced catalytic activity, but also improved catalyst durability for the ORR. Figure 5 summarizes the electrochemical results for the PtNi/C catalysts before and after 4000 potential cycles between 0.6 and 1.1 V at 60 °C. Both the acid treated and the acid treated/annealed PtNi/C catalysts had minor losses (∼10%) in ECSA after cycling, in comparison to a substantial drop (∼40%) for Pt/C (Figure 5a). An additional observation was that the acid treated/annealed PtNi/C had only 15% loss in specific activity, in contrast to 57% for the acid treated catalyst and 38% for Pt/C (Figure 5b). We have also applied in situ XANES to monitor the catalyst structures in the durability studies (Figure 5d and e, and more details in the Supporting Information). Not surprisingly, the acid treated/annealed PtNi/C does not show visible changes, whereas reduction of absorption at the Ni edge was observed for the acid treated PtNi/C during and after potential cycling. These findings are in line with the elemental analysis of the PtNi/C catalysts after the durability experiments, which indicate no loss for the Ni content in the acid treated/annealed catalyst in contrast to the significant loss of Ni in the acid treated catalyst (Figures S5). It is thus assured that the multilayered Pt-skin formation has indeed provided complete protection of the Ni inside the catalyst and enabled the sustained high catalytic activity under fuel cell operating conditions. On the basis of that, in addition to diminished number of vulnerable undercoordinated Pt surface atoms after annealing, multilayered Pt-skin formation is also thick enough to protect subsurface Ni from dissolution that otherwise occurs through the place-exchange mechanism[12a] (Figures 5 and S5). At the same time,


dx.doi.org/10.1021/ja2047655 |*J. Am. Chem. Soc.* 2011, 133, 14396–14403

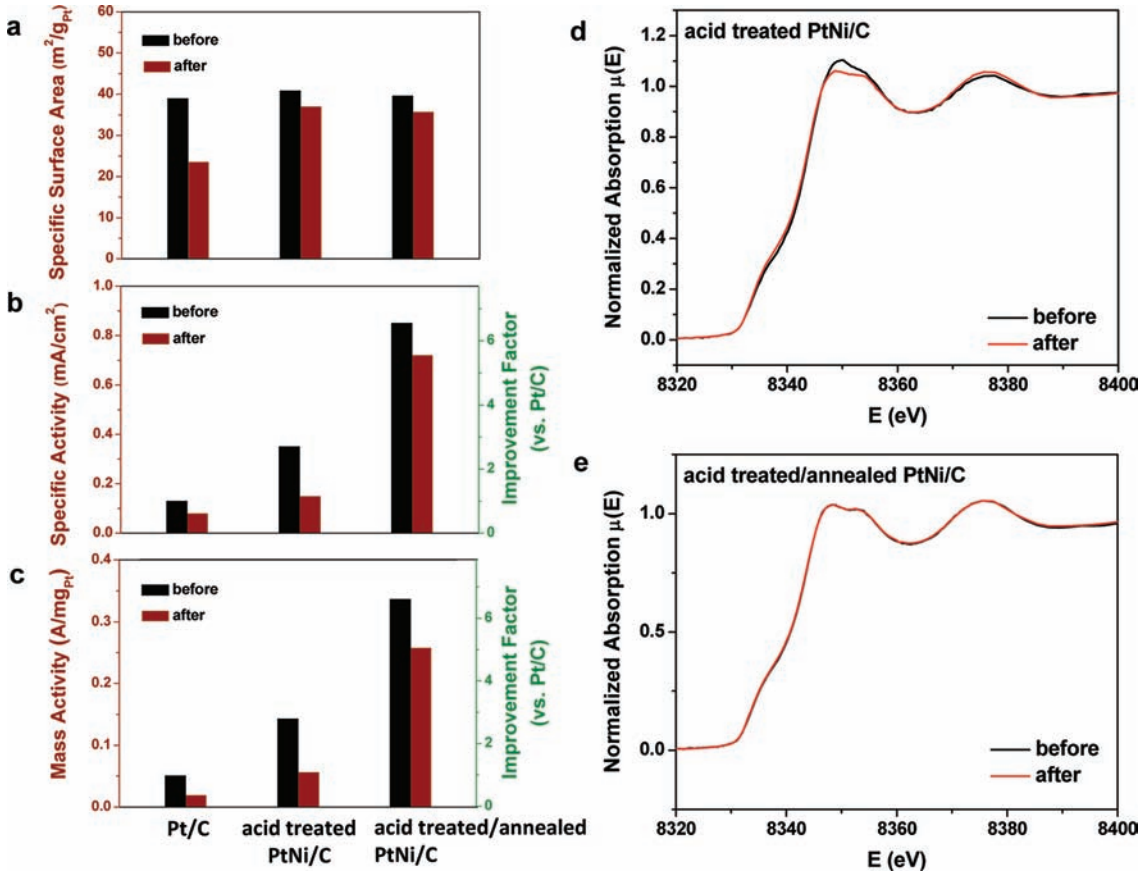


**Figure 5.** Summary of electrochemical durability studies obtained by RDE before and after 4000 potential cycles between 0.6 and 1.1 V for the Pt/C and PtNi/C catalysts in 0.1 M $HClO_4$ at 0.95 V and 60 °C: (a) specific surface area, (b) specific activity, and (c) mass activity. Activity improvement factors versus Pt/C before and after cycling were also shown for specific and mass activities in (b) and (c). Parts (d) and (e) show the XANES spectra recorded for the acid treated and acid treated/annealed PtNi/C catalysts at Ni K edge, at 1.0 V before and after potential cycling. Estimation of ECSA was based on integrated $H_{upd}$ for the Pt/C and acid treated PtNi/C catalysts, and $CO_{ad}$ stripping polarization curve for the acid treated/annealed PtNi/C catalyst.

the multilayered Pt-skin is thin enough to maintain typical skin-like properties (discussed above), which originates from altered electronic structures due to the presence of a desirable amount of subsurface Ni. As a result, the PtNi/C catalyst with multilayered Pt-skin surfaces exhibited improvement factors in mass activity of more than 1 order of magnitude after elongated potential cycling versus the Pt/C catalyst (Figure 5c).

## SUMMARY

We have demonstrated the design and synthesis of an advanced Pt−bimetallic catalyst, which simultaneously achieves high catalytic activity and superior durability for the ORR. The developed catalyst contains a unique nanoscale architecture with a PtNi core of 50 at% Ni and a multilayered Pt-skin surfaces. This structure was built up through synergistic studies of extended surfaces and nanocatalysts, with critical parameters such as particle size, thermal treatment, particle sintering, alloy composition, and elemental composition profile integrally designed and optimized. Delicate structure−function correlation in the bimetallic electrocatalysts with composite nanostructures has been comprehensively resolved by employing state-of-the-art electron microscopy and *in situ* X-ray spectroscopy characterization. Our findings have immense implications for the development of heterogeneous catalysts and nanostructure engineering toward advanced functional materials.

## ASSOCIATED CONTENT

**Supporting Information.** Additional material characterization and theoretical analysis. This material is available free of charge via the Internet at http://pubs.acs.org.

## AUTHOR INFORMATION

**Corresponding Author**
vrstamenkovic@anl.gov

## ACKNOWLEDGMENT

This work was conducted at Argonne National Laboratory, a U.S. Department of Energy, Office of Science Laboratory, operated by UChicago Argonne, LLC, under contract no. DE-AC02-06CH11357. It was sponsored by the U.S. Department of Energy, Office of Energy Efficiency and Renewable Energy, Fuel Cell Technologies Program. Microscopy research was conducted

at the Electron Microscopy Center for Materials Research at Argonne, and ORNL's SHaRE User Facility sponsored by the Scientific User Facilities Division, Office of Basic Energy Sciences, the U.S. Department of Energy. XANES were accomplished at the Advanced Photon Source at Argonne. We thank Dr. Cindy Chaffee for the help on setup at APS, and Dr. Sonke Seifert and Byeongdu Lee from APS for valuable discussion on X-ray absorption experiments.

## REFERENCES

(1) Vielstich, W.; Lamm, A.; Gasteiger, H. A. *Handbook of Fuel Cells: Fundamentals, Technology, and Applications*; Wiley: Chichester, England; Hoboken, NJ, 2003; p 4.

(2) (a) Abraham, K. M.; Jiang, Z. *J. Electrochem. Soc.* **1996**, *143*, 1–5. (b) Armand, M.; Tarascon, J. M. *Nature* **2008**, *451*, 652–657.

(3) Gasteiger, H. A.; Kocha, S. S.; Sompalli, B.; Wagner, F. T. *Appl. Catal., B* **2005**, *56*, 9–35.

(4) (a) Stamenkovic, V.; Mun, B. S.; Mayrhofer, K. J. J.; Ross, P. N.; Markovic, N. M.; Rossmeisl, J.; Greeley, J.; Norskov, J. K. *Angew. Chem., Int. Ed.* **2006**, *45*, 2897–2901. (b) Stamenkovic, V. R.; Mun, B. S.; Arenz, M.; Mayrhofer, K. J. J.; Lucas, C. A.; Wang, G. F.; Ross, P. N.; Markovic, N. M. *Nat. Mater.* **2007**, *6*, 241–247.

(5) Stamenkovic, V. R.; Mun, B. S.; Mayrhofer, K. J. J.; Ross, P. N.; Markovic, N. M. *J. Am. Chem. Soc.* **2006**, *128*, 8813–8819.

(6) Stamenkovic, V. R.; Fowler, B.; Mun, B. S.; Wang, G. F.; Ross, P. N.; Lucas, C. A.; Markovic, N. M. *Science* **2007**, *315*, 493–497.

(7) (a) Strasser, P.; Mani, P.; Srivastava, R. *J. Phys. Chem. C* **2008**, *112*, 2770–2778. (b) Chen, S.; Sheng, W. C.; Yabuuchi, N.; Ferreira, P. J.; Allard, L. F.; Shao-Horn, Y. *J. Phys. Chem. C* **2009**, *113*, 1109–1125. (c) Chen, J. Y.; Lim, B.; Lee, E. P.; Xia, Y. N. *Nano Today* **2009**, *4*, 81–95. (d) Zhang, J.; Yang, H. Z.; Fang, J. Y.; Zou, S. Z. *Nano Lett.* **2010**, *10*, 638–644. (e) Strasser, P.; Koh, S.; Anniyev, T.; Greeley, J.; More, K.; Yu, C. F.; Liu, Z. C.; Kaya, S.; Nordlund, D.; Ogasawara, H.; Toney, M. F.; Nilsson, A. *Nat. Chem.* **2010**, *2*, 454–460.

(8) (a) Wang, C.; Wang, G. F.; van der Vliet, D.; Chang, K. C.; Markovic, N. M.; Stamenkovic, V. R. *Phys. Chem. Chem. Phys.* **2010**, *12*, 6933–6939. (b) Schulenburg, H.; Muller, E.; Khelashvili, G.; Roser, T.; Bonnemann, H.; Wokaun, A.; Scherer, G. G. *J. Phys. Chem. C* **2009**, *113*, 4069–4077.

(9) (a) van Hardeveld, R.; Hartog, F. *Surf. Sci.* **1969**, *15*, 189–230. (b) Kinoshita, K. *J. Electrochem. Soc.* **1990**, *137*, 845–848.

(10) (a) Han, B. C.; Miranda, C. R.; Ceder, G. *Phys. Rev. B* **2008**, *77*, 075410. (b) Strmcnik, D. S.; Tripkovic, D. V.; van der Vliet, D.; Chang, K. C.; Komanicky, V.; You, H.; Karapetrov, G.; Greeley, J.; Stamenkovic, V. R.; Markovic, N. M. *J. Am. Chem. Soc.* **2008**, *130*, 15332–15339.

(11) (a) Mayrhofer, K. J. J.; Blizanac, B. B.; Arenz, M.; Stamenkovic, V. R.; Ross, P. N.; Markovic, N. M. *J. Phys. Chem. B* **2005**, *109*, 14433–14440. (b) Wang, C.; van der Vilet, D.; Chang, K. C.; You, H. D.; Strmcnik, D.; Schlueter, J. A.; Markovic, N. M.; Stamenkovic, V. R. *J. Phys. Chem. C* **2009**, *113*, 19365–19368.

(12) (a) Komanicky, V.; Chang, K. C.; Menzel, A.; Markovic, N. M.; You, H.; Wang, X.; Myers, D. *J. Electrochem. Soc.* **2006**, *153*, B446–B451. (b) Borup, R.; et al. *Chem. Rev.* **2007**, *107*, 3904–3951.

(13) Wang, C.; Chi, M.; Wang, G.; van der Vliet, D.; Li, D.; More, K.; Wang, H.-H.; Schlueter, J. A.; Markovic, N. M.; Stamenkovic, V. R. *Adv. Funct. Mater.* **2011**, *21*, 147–152.

(14) Beno, M. A.; Engbretson, M.; Jennings, G.; Knapp, G. S.; Linton, J.; Kurtz, C.; Rutt, U.; Montano, P. A. *Nucl. Instrum. Methods Phys. Res., Sect A* **2001**, *467*, 699–702.

(15) Newville, M.; Livins, P.; Yacoby, Y.; Rehr, J. J.; Stern, E. A. *Phys. Rev. B* **1993**, *47*, 14126–14131.

(16) (a) Newville, M. *J. Synchrotron Radiat.* **2001**, *8*, 322–324. (b) Ravel, B.; Newville, M. *J. Synchrotron Radiat.* **2005**, *12*, 537–541.

(17) (a) Newman, J. *J. Electrochem. Soc.* **1966**, *113*, 2. (b) van der Vliet, D.; Strmcnik, D. S.; Wang, C.; Stamenkovic, V. R.; Markovic, N. M.; Koper, M. T. M. *J. Electroanal. Chem.* **2010**, *647*, 29–34.

(18) Ahrenstorf, K.; Heller, H.; Kornowski, A.; Broekaert, J. A. C.; Weller, H. *Adv. Funct. Mater.* **2008**, *18*, 3850–3856.

(19) Kiely, C. J.; Fink, J.; Brust, M.; Bethell, D.; Schiffrin, D. J. *Nature* **1998**, *396*, 444–446.

(20) Li, Y.; Zhang, X. L.; Qiu, R.; Qiao, R.; Kang, Y. S. *J. Phys. Chem. C* **2007**, *111*, 10747–10750.

(21) Bunker, G. *Introduction to XAFS: A Practical Guide to X-ray Absorption Fine Structure Spectroscopy*; Cambridge University Press: Cambridge, UK; New York, 2010; viii, 260 pp.

(22) (a) Mukerjee, S.; Srinivasan, S.; Soriaga, M. P.; Mcbreen, J. *J. Electrochem. Soc.* **1995**, *142*, 1409–1422. (b) Rodriguez, J. A.; Hanson, J. C.; Frenkel, A. I.; Kim, J. Y.; Perez, M. *J. Am. Chem. Soc.* **2002**, *124*, 346–354.

(23) (a) Imai, H.; Izumi, K.; Matsumoto, M.; Kubo, Y.; Kato, K.; Imai, Y. *J. Am. Chem. Soc.* **2009**, *131*, 6293–6300. (b) Friebel, D.; Miller, D. J.; O'Grady, C. P.; Anniyev, T.; Bargar, J.; Bergmann, U.; Ogasawara, H.; Wikfeldt, K. T.; Pettersson, L. G. M.; Nilsson, A. *Phys. Chem. Chem. Phys.* **2011**, *13*, 262–266. (c) Russell, A. E.; Rose, A. *Chem. Rev.* **2004**, *104*, 4613–4635.